ELSEVIER

Contents lists available at ScienceDirect

Journal of Non-Crystalline Solids

journal homepage: www.elsevier.com/locate/jnoncrysol





Effect of cryogenic cycling and above- T_g annealing on the corrosion behavior of Zr-Cu-Ti-Be metallic glass

Akib Jabed*, Golden Kumar

Department of Mechanical Engineering, The University of Texas at Dallas, Richardson, TX 75080, USA

ARTICLE INFO

Keywords: Metallic glass Electrochemistry Cryogenic treatment Isothermal annealing

ABSTRACT

This work investigates the electrochemical properties of Zr-based $\rm Zr_{35}Ti_{30}Cu_{8.25}Be_{26.75}$ metallic glass after cryogenic treatment and isothermal annealing above glass transition temperature. Potentiodynamic polarization and electrochemical impedance spectroscopy experiments are used to understand the effect of structural state on the corrosion behavior of Zr-based metallic glass. The metallic glass samples are cycled between liquid nitrogen to room temperature and isothermally held at liquid nitrogen to unravel the effect of cryogenic treatments on the electrochemical properties. The corrosion of cryogenically treated and high temperature annealed samples is compared with the as-cast samples. The results show that holding at liquid nitrogen temperature improves the corrosion resistance of metallic glass compared to cryogenic cycling and the high temperature annealing. These findings are explained based on the changes in structural state of metallic glass.

1. Introduction

Metallic glasses (MGs) are known for their high strength, large elasticity, and good wear resistance resulting from the homogeneous amorphous structure [1–3]. Among many glass forming metal systems, Zr-based alloys have attracted more attention because of their high glass forming ability, large supercooled liquid temperature range, and lower material cost [4,5]. These traits are particularly desirable for potential applications of MGs, which have suffered from size and cost limitations. MGs are considered for applications in bio-implants, gearboxes for space missions, sports goods, and precision metal parts [6-9]. The chemical stability of MG in the service environment is also a critical factor in evaluating its applicability for a specific application. MGs typically exhibit enhanced corrosion resistance compared to their crystalline counterparts due to absence of pit nucleation sites such as grain boundaries and chemical heterogeneities. However, the corrosion of MGs is sensitive to their composition and the type of chemical environment [10-12].

Extensive corrosion studies have been conducted on different Zr-based glass forming compositions such as Zr-Cu-Ni-Al, Zr-Cu-Fe-Al-Ag, and Zr-Cu-Ti-Ni-Be [13–17]. Biocorrosion of Zr-based MGs free of toxic elements has also received great attention because of potential applications in implants. The corrosion of Zr-based MGs has been studied in acidic and alkaline electrolytes with varying pH values to mimic the

It is well known that the structural changes induced by annealing strongly affect the mechanical and corrosion properties of MGs. Structural relaxation during annealing below glass transition temperature (T_g) results in improved corrosion resistance due to annihilation of free volume [10,30,31]. The effect of above- T_g annealing on corrosion of MGs is less consistent and it varies with alloy composition and the extent of crystallization. Both decrease and increase in corrosion resistance after annealing above- T_g have been reported in different MGs [32-34]. Recent studies have shown that the plasticity of MGs is improved by structural rejuvenation through thermal cycling between cryogenic and elevated temperatures [2,35]. These findings have spurred interest in corrosion testing of MGs subjected to cryogenic temperatures [32,36,37]. The effect of cryogenic exposure on MGs is also important for their

E-mail address: akib.jabed@utdallas.edu (A. Jabed).

service conditions [18–20]. The enhanced corrosion resistance of Zr-based MGs is generally attributed to the ability of Zr to form an oxide layer which serves as a passivation layer against adverse electrochemical reaction. As a result, the Zr-based MGs display effective corrosion resistance in mediums containing chloride, sulfate, and hydroxide ions [3,6,21,22]. The resistance against chloride ions (Cl⁻) is particularly attractive because Cl⁻easily propagates through grain boundaries in crystalline metals [22–24]. The corrosion resistance of MGs towards specific chemicals can be tailored to some extent by varying the alloying elements [25–28]. Passivation layer formation in NaCl solution is promoted by addition of Nb, Co, Ta, and Cr in Zr-based MGs [29].

 $^{^{\}ast}$ Corresponding author.

potential use in space applications. Gu et al. [32] showed that cryogenic cycling results in decrease in corrosion resistance of Ti-Zr-Be-Ni MG due to redistribution of free volume. However, Zhao et al. [37] reported significant improvement in the corrosion performance of Ni-Nb-Zr MG after holding at -100 °C due to reduction in structural heterogeneity. Currently, there is insufficient data to draw unambiguous conclusions about the influence of cryogenic treatment and exposure on the corrosion properties of MGs. In this study, the effects of cryogenic cycling and holding, and above- T_g annealing on the corrosion properties of $\rm Zr_{35}Ti_{30}Cu_{8.25}Be_{26.75}\,MG$ are investigated.

2. Experimental procedure

Zr₃₅Ti₃₀Cu_{8.25}Be_{26.75} MG (hereafter referred as Zr-MG) cylindrical rod of about 10 mm diameter was acquired from Liquidmetal Technologies. The T_g and T_x (crystallization onset temperature) of as-cast Zr-MG measured using differential scanning calorimetry (DSC) were 300°C and 450°C, respectively. Small MG pieces were thermoplastically formed into 15 mm diameter discs with a thickness of 0.5 mm. The discs were subjected to three different structural treatments and their corrosion performance was compared with an untreated reference disk (labeled as AC). The Zr-MG discs were isothermally annealed above T_g , cycled between liquid nitrogen and room temperature, and held at liquid nitrogen temperature to induce varying structural changes. Above- T_g annealing was performed at 410°C for 5 min (labeled as A1) and 12 min (labeled as A2) whereas the onset time for crystallization at 410°C is 17 min. For cycling experiments, the Zr-MG discs were submerged in liquid nitrogen for 1 min followed by 5 min holding in air to reach room temperature.

These thermal cycles were repeated 10 times (labeled as C1) and 30 times (labeled as C2). To further evaluate the effect of cryogenic exposure on corrosion, the MG discs were submerged in liquid nitrogen for 30 min (labeled as CT1) and 300 min (labeled as CT2).

The corrosion properties of Zr-MG samples after different thermal treatments were characterized using a Gamry 1010E Potentiostat with three-electrode cell at room temperature. All samples were polished to obtain comparable surface roughness before corrosion testing. The MG sample was used as the working electrode and a graphite rod and a saturated calomel electrode (SCE) were used as the counter and the reference electrodes, respectively. The corrosion performance in 3.5 wt. % NaCl electrolyte was evaluated using open circuit potential (OCP), potentiostatic electrochemical impedance spectroscopy (EIS) and potentiodynamic polarization experiments by exposing 1 cm² area of MG discs. The OCP measurements were performed for 60 min to reach a nearly stabilized potential. The EIS tests were conducted at an AC voltage of 10 mV up to a frequency of 0.01 Hz to understand the passivation behavior of MG specimens. The potentiodynamic polarization tests were performed within a range of -0.5 V/OCP to 1.5 V/OCP at a scan rate of 1 mV/s.

3. Results and discussion

The following sections describe the effect of different thermal treatments on the thermal and the electrochemical behavior of Zr-MG.

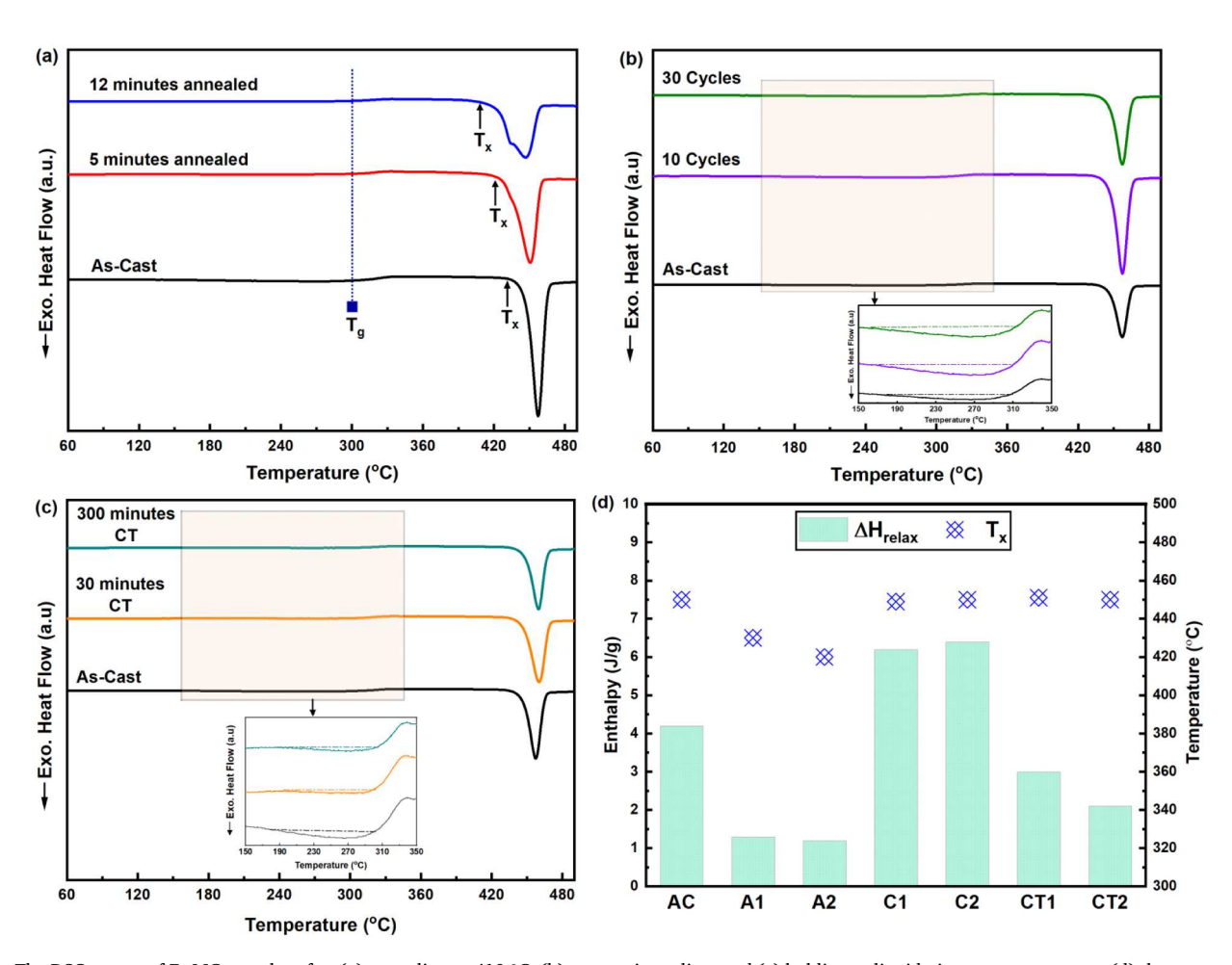


Fig. 1. The DSC curves of Zr-MG samples after (a) annealing at 410 $^{\circ}$ C, (b) cryogenic cycling, and (c) holding at liquid nitrogen temperature. (d) the comparison of ΔH_{relax} and T_x values for Zr-MG samples after different structural treatments.

3.1. Thermal characterization

The structural changes in Zr-MG samples after different thermal treatments are analyzed using DSC. The DSC curves measured at a constant heating rate of 20° C/min for all the samples are shown in Fig. 1. In above- T_g annealed samples, the onset temperature and enthalpy of crystallization decrease with increasing annealing time whereas the T_g remains unaffected (Fig. 1a). These observations are typical for partially crystallized MGs indicating the progression in crystallization during above- T_g annealing [38]. The maximum fraction of crystalline phase estimated from the enthalpy of crystallization is about 20% for A2 sample [39]. The experimental studies have shown that the size of crystals is in the range 5–15 nm during isothermal annealing of Zr-based MGs [40]. These nanocrystals are homogenously distributed in isothermally annealed MG samples [40].

The effect of cycling between the liquid nitrogen and room temperature on DSC curves of Zr-MG is shown in Fig. 1b. While the T_g and the T_x are not affected by cryogenic cycling, an additional exothermic event before T_g is observed as shown in the inset of Fig. 1b. Such a broad exothermic peak below T_g in cryogenically cycled MGs is attributed to relaxation of structural disorder generated during thermal cycling [35, 36]. The area of exothermic peak (ΔH_{relax}) increased with number of thermal cycles from 10 to 30 (Fig. 1b). The ΔH_{relax} values were calculated as 4.93 J/g, 6.17 J/g, and 6.47 J/g for the AC, C1, and C2 samples, respectively. It has been shown that the structural rejuvenation through thermal cycling in MGs reaches saturation after a certain number of cycles [35]. A smaller change in ΔH_{relax} values from 10 to 30 cycles suggests that the structural rejuvenation is close to saturation in Zr-MG.

The DSC curves of samples isothermally held at liquid nitrogen are shown in Fig. 1c. The exothermic peak corresponding to structural relaxation before T_g reduces in the cryogenically treated samples. The absence of exothermic events in CT1 and CT2 samples indicates that longer holding at cryogenic temperatures creates an opposite effect to that of cryogenic cycling. The structural disorder redistributes, and the MG becomes more homogenous after holding at cryogenic temperature. To compare the effects of all three thermal treatments on structure of Zr-MG, ΔH_{relax} and T_x values are plotted in Fig. 1d. It is observed that the ΔH_{relax} increases with cryogenic cycling but diminishes upon long term exposure to cryogenic environment. In contrast, the T_x is only affected by annealing in the supercooled liquid state due to partial crystallization. Therefore, the cryogenically cycled MG samples exhibit maximum structural rejuvenation which is consistent with enhanced plasticity

reported in literature [2,35].

3.2. Electrochemical characterization

Open circuit potential (OCP), potentiostatic EIS and potentiodynamic polarization experiments were conducted to evaluate the effects of different thermal treatments on the corrosion properties of Zr-MG.

3.2.1. Open circuit potential

The OCP indicates the stability of a sample in an environment without AC or DC current. Every sample when tested using OCP will have a specific potential depending on the composition of electrolyte, the testing temperature, the sample chemistry, and the surface quality. The potential obtained in OCP experiments is not the inherent property of material but varies with the structure. To achieve the stabilizing potential for Zr-MG samples with different structures, the OCP data was recorded for 60 min. The trend of OCP for each sample is shown in Fig. 2a. The OCP values show a transition towards less negative value for all the samples except C2 for which the OCP changes from -0.41 V to -0.42 V after 60 min (Fig. 2b). These observations indicate the dissolution of the passive layer for the C2 sample, whereas the ongoing passivation with time for the other samples. The CT1 and CT2 samples show the lowest final voltages of -0.38 V and -0.36 V, respectively. These results suggest that the samples held at cryogenic temperature form a dense passivation layer. The less dense passivation layer in the cryogenically cycled C2 sample may be attributed to the presence of structural heterogeneity, whereas partial crystallization is likely responsible for the poor passivation in the A1 sample [34].

The significant amounts of Zr- and Ti- (65 at.% combined) in $\rm Zr_{35}Ti_{30}Cu_{8.25}Be_{26.75}$ alloy are beneficial due to the ability of these elements to form an oxide layer over a wide range of potential-pH diagram [6]. In addition, the presence of Cu with a positive standard reduction potential (+ 0.09 V vs SCE) may also contribute towards the passivation of Zr-MG [6]. Therefore, the OCP experiments can provide a valuable insight into the electrochemical behavior, however, EIS and polarization analyses are required to obtain a complete understanding of corrosion mechanism.

3.2.2. Potentiostatic EIS

The Bode and Nyquist plots for different Zr-MG samples achieved from EIS experiments are shown in Fig. 3. The data extracted from these plots using circuit model fitting are listed in Table 1. The Bode plot

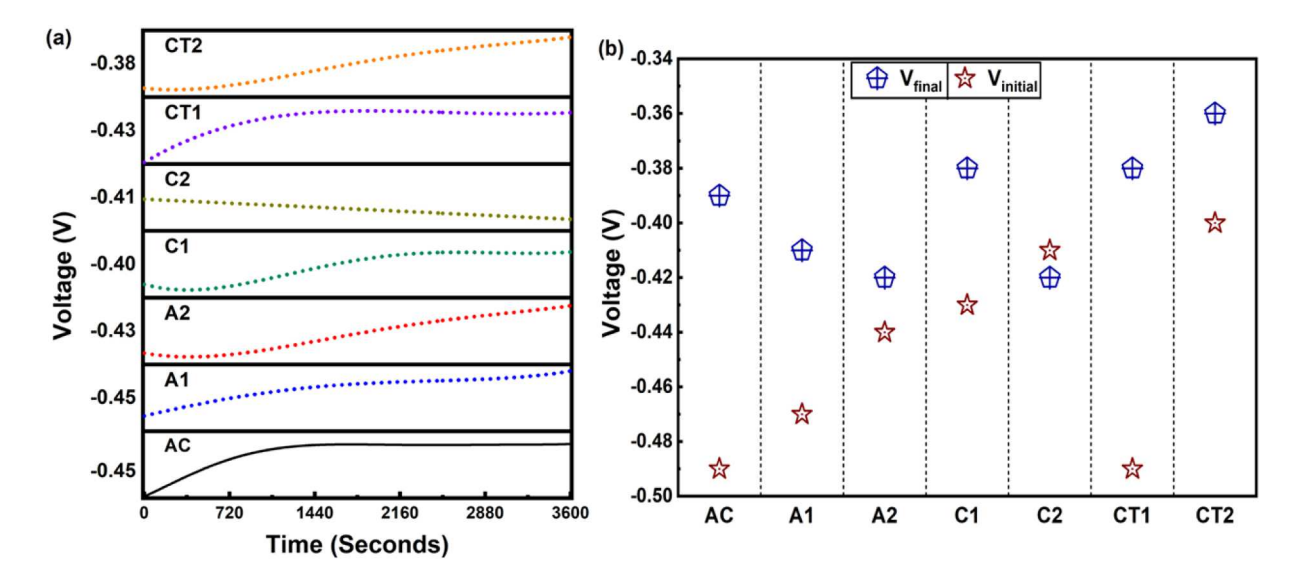


Fig. 2. Open Circuit Potential (OCP) of Zr-MG samples after different structural treatments. (a) The change in OCP as a function of time. (b) The initial and final voltage values achieved from the OCP curves for each sample.

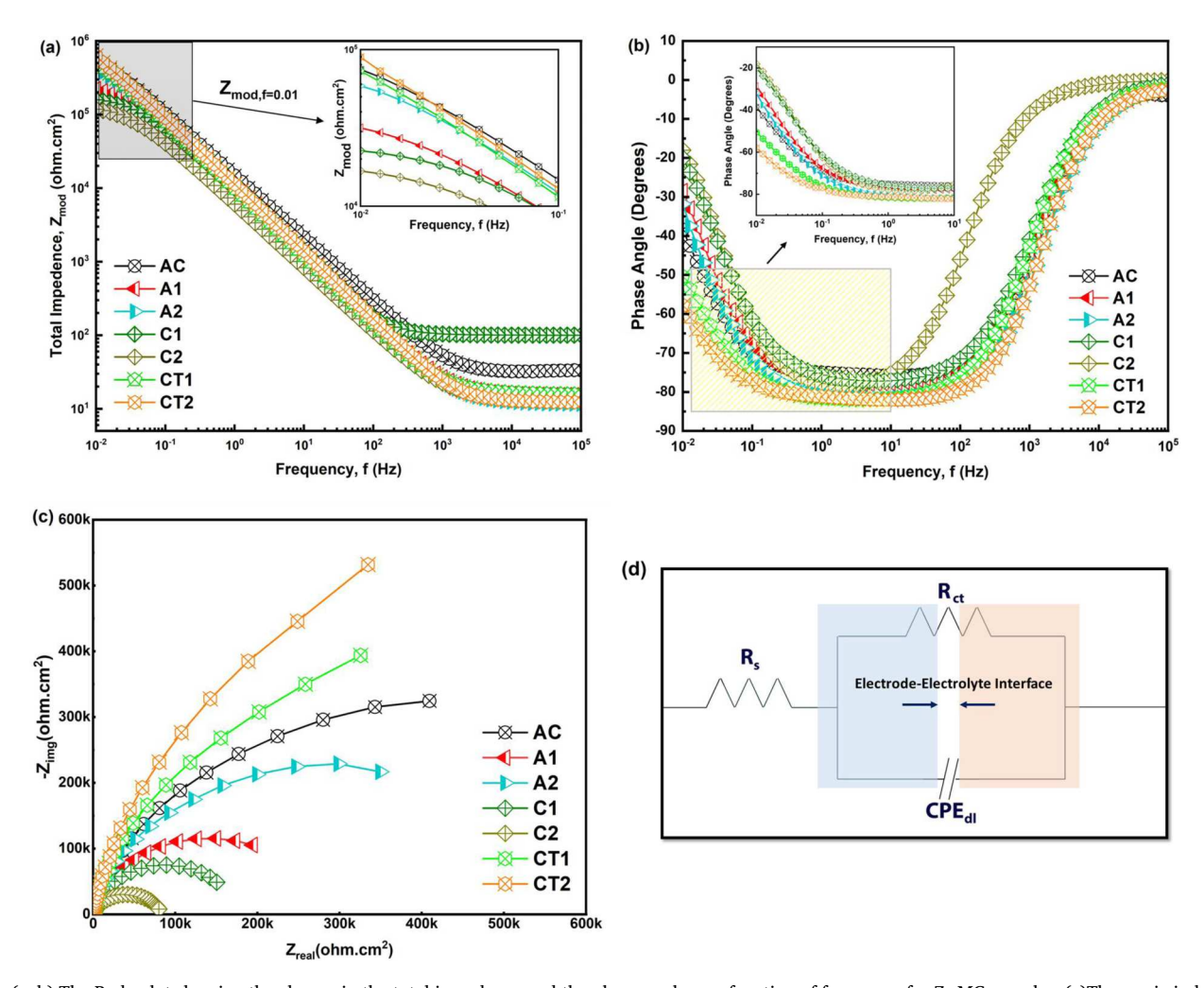


Fig. 3. (a–b) The Bode plot showing the change in the total impedance and the phase angle as a function of frequency for Zr-MG samples. (c) The semi-circle in the Nyquist plot reflecting the charge transfer resistance of Zr-MG samples. (d) The R_s -(CPE)_{dl}- R_{ct} equivalent circuit model used to extract the charge transfer resistance and the active surface area.

Table 1Corrosion parameters extracted from the EIS and Potentiodynamic polarization curves.

Samples	Corrosion Potential E _{corr}	Pitting Potential E _{pit}	Passive Domain ΔE	Corrosion Current Density	Passive current density	Charge Transfer Resistance R _{ct}	Double Layer Capacitance CPE _{dl}	
	[V vs. SCE]	[V vs. SCE]	[V vs. SCE]	¹ corr [μA.cm ⁻²]	^I pass [μA.cm ⁻²]	$[M\Omega$ -cm ²]	$Q \\ [\mu\Omega^{-1}s^{-n}cm^{-2}]$	α
AC	-0.5 ± 0.11	-0.29 ± 0.13	0.21	0.22	1.40	0.57	18.87	0.92
A1	-0.47 ± 0.11	$-0.34 {\pm} 0.16$	0.13	0.35	1.13	0.23	24.02	0.87
A2	$-0.45 {\pm} 0.12$	-0.29 ± 0.10	0.16	0.23	1.91	0.28	20.05	0.89
C1	$-0.43 {\pm} 0.08$	$-0.31 {\pm} 0.12$	0.11	0.82	1.42	0.17	24.79	0.88
C2	-0.48 ± 0.13	-0.36 ± 0.11	0.12	3.11	18.7	0.08	33.13	0.86
CT1	-0.44 ± 0.15	$-0.27 {\pm} 0.05$	0.17	0.19	0.89	0.64	18.10	0.92
CT2	$-0.42 {\pm} 0.06$	$-0.15 {\pm} 0.12$	0.27	0.17	0.94	0.76	17.38	0.91

reveals the relationship between the impedance (Z) and the frequency response of a system. Fig. 3a shows the total impedance ($\rm Z_{mod,f=0.01}$) in the lower frequency region. The higher value of impedance usually indicates better corrosion resistance. The impedance is higher for the CT2 (0.63 $\rm M\Omega\text{-cm}^2$) and CT1 (0.52 $\rm M\Omega\text{-cm}^2$) compared to the as-cast sample AC (0.51 $\rm M\Omega\text{-cm}^2$), which indicates improved stability of passivation layer against ion dissolution in cryogenically treated samples. In contrast, the C1 and C2 specimens show lower impedance values of 0.16 $\rm M\Omega\text{-cm}^2$ and 0.12 $\rm M\Omega\text{-cm}^2$, respectively. The above- T_g annealed samples also exhibit low impedance values of 0.22 $\rm M\Omega\text{-cm}^2$ for A1 and 0.43 $\rm M\Omega\text{-cm}^2$ for A2. Thus, the total impedance data indicate that holding at

cryogenic temperature results in better corrosion resistance than cryogenic cycling and above- T_g annealing. The corrosion resistance of above- T_g annealed samples is superior to the cryogenically cycled samples.

The Nyquist plot was used to further verify the trend observed in electrochemical properties of thermally treated Zr-MG samples (Fig. 3c). The slope in Nyquist plot is an indicator of charge transfer resistance ($R_{\rm ct}$) and a higher value indicates better protection against harmful chemical reactions [41]. It can be observed from Fig. 3c that the cryogenically treated samples display a higher slope compared to the untreated sample whereas the cycled and above- T_g annealed specimens show a lower slope. The EIS curves were fitted using an equivalent

circuit to obtain the values of $R_{ct}.$ According to the Bode plot (Fig. 3b), the data from Zr-MG samples can be described by a single time constant and phase angle smaller than $90^{\circ}.$ Thus, the $R_{s}\text{-}(\text{CPE}_{dl})\text{-}R_{ct}$ circuit model as shown in Fig. 3d is appropriate to extract the essential EIS parameters. Here, R_{s} is the solution resistance and CPE $_{dl}$ is the double layer capacitance between the electrolyte and the working electrode. The impedance of a double layer capacitance ($Z_{\text{CPE}_{dl}}$) is usually represented using following equation:

$$Z_{CPE_{dl}} = \frac{1}{iO\omega^{\alpha}}$$

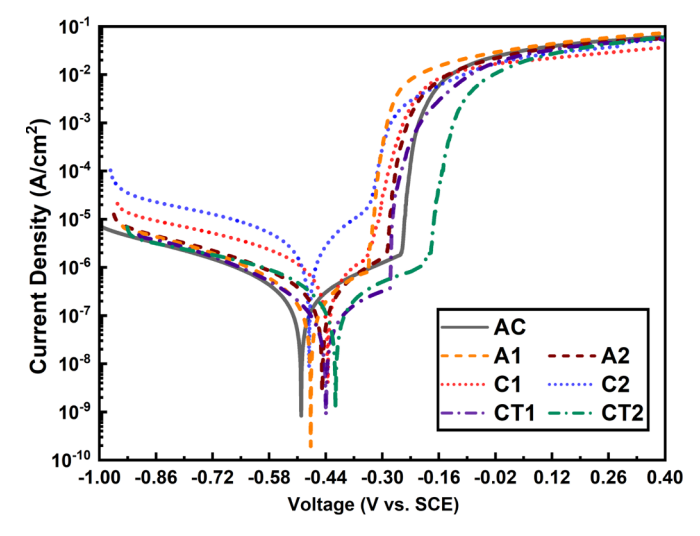
Where Q is the pseudo capacitance of the system, ω is the angular frequency, and α is dispersion coefficient associated with surface heterogeneity. The values of all these parameters extracted by fitting the EIS curves are provided in Table 1. The R_{ct} is higher for the cryogenically treated samples compared to the cycled and above- T_g annealed samples. These findings are consistent with the Nyquist plot. The CT2 sample has the highest R_{ct} of 0.76 $M\Omega$ -cm². The reduced R_{ct} in the cryogenically cycled and annealed MG samples is attributed to the increased structural heterogeneity. In contrast, long term cryogenic exposure results in more homogeneous MG with higher corrosion resistance. It is worth noting that the corrosion resistance improves with annealing time in above- T_g heated samples indicated by higher R_{ct} and lower Q values for A2 compared to A1 sample. These results indicate that the structure of MG is more heterogeneous in the early stage of crystallization, and therefore, more prone to corrosion. This is reasonable because the microstructural homogeneity improves as the crystallization progresses towards completion with annealing time. The corrosion parameters listed in Table 1 reveal that the quality of passivation layer and the corrosion resistance of MGs depend on the structural homogeneity. The structure of MGs after cryogenic cycling is more heterogenous resulting in least corrosion resistance.

The parameters associated with $Z_{\text{CPE}_{\text{dl}}}$ can also be used to further analyze the corrosion properties of Zr-MG samples. The value of α close to 1 indicates better capacitive behavior to protect the sample surface. The CT1, CT2 and AC samples have higher α value (Table 1), indicating the reaction area of these samples has reduced compared to the annealed and the cryogenically cycled samples. The reduction in reaction area lowers the probability of harmful electrochemical reactions due to the formation of stable passive layer. The compactness of the passive film is further supported by the lower value of Q in CT2 (17.38 $\mu\Omega^{-1}$ s⁻ⁿcm⁻²) and CT1 (18.10 $\mu\Omega^{-1}s^{-n}cm^{-2}$) samples compared to C2 (33.13 $\mu\Omega^{-1}s^{-n}cm^{-2}$), C1(24.79 $\mu\Omega^{-1}s^{-n}cm^{-2}$), A1 (24.02 $\mu\Omega^{-1}s^{-n}cm^{-2}$), A2 (20.05 $\mu\Omega^{-1} s^{-n} cm^{-2}$) as well as AC (18.87 $\mu\Omega^{-1} s^{-n} cm^{-2}$) samples. The lower value of Q in CT2 and CT1 samples compared to the other sample verifies the formation of dense protective layer in cryogenically treated samples. To further understand the effect of passivation behavior on the electrochemical features of Zr-MG, polarization tests were performed, and the results are discussed in the following section.

3.2.3. Potentiodynamic polarization

The electrochemical behavior of Zr-MG samples subjected to different treatments is evaluated using the potentiodynamic polarization experiments (Fig. 4). The results indicate increasing passivation with time in the anodic region of the polarization curve. In addition, sudden increase of the current density is observed at a specific potential upon upward scanning in the anodic polarization curve, which is typically identified as the pitting potential [32]. Crucial electrochemical parameters such as corrosion potential (E_{corr}), pitting potential (E_{pit}), width of passive region ($\Delta E=E_{pit}$ - E_{corr}), corrosion current density (I_{corr}), and passivation current density (I_{pass}) are extracted from the polarization curves using Tafel extrapolation (Table 1). The polarization data reveals a striking contrast in the corrosion resistance of Zr-MG samples despite identical polarization behavior.

The higher E_{corr} in the polarization experiments is usually indicative of better resistance towards corrosion. The E_{corr} is maximum for the



 $\textbf{Fig. 4.} \ \ \textbf{The Potentiodynamic polarization plots for the Zr-MG samples after different thermal treatments.}$

cryogenically treated sample CT2 (-0.42 V), whereas the least value is detected for the as-cast sample AC (-0.5 V). The cryogenically treated sample also exhibits higher E_{pit} (-0.15 V for CT2 sample) compared to the other samples, which indicates higher resistance against pit initiation after cryogenic holding. The elevated pit nucleation resistance in CT2 sample can be attributed to better passivation observed in the anodic polarization curve. The passive region (ΔE) with a maximum width (-0.27 V) is observed in CT2 sample, whereas the cryogenically cycled samples show lower ΔE (-0.11 V). The smaller ΔE in the cycled samples indicates that an increased structural heterogeneity has a negative impact on the passivation behavior.

The effect of passivation is also observed in the corrosion rate of the samples, which is usually quantified using the I_{corr} and I_{pass} of the polarization curve. The MG sample subjected to 30 cryogenic cycles has a higher I_{corr} (3.11 $\mu A.cm^{-2}$ for C2), suggesting higher dissolution rate. Similar trend is also observed for the passivation current density and C2 sample exhibits higher I_{pass} of 18.7 $\mu A.cm^{-2}$. Notably, no substantial difference in the corrosion and passive current densities is detected for the other samples and the I_{corr} and I_{pass} are in the order of $10^{-6}~\mu A.cm^{-2}$ with comparable range of quantitative values. The critical electrochemical parameters suggest that the higher number of cryogenic cycles result in poor corrosion resistance.

Fig. 5 shows the morphologies of Zr-MG samples after potentiodynamic polarization experiments. Randomly formed round pits are visible with an average diameter of about 15 μ m for the as-cast and the sample annealed above- T_g for 12 min (Fig. 5a and b). The pit diameter increased alongside "wear-furrow" features in cryogenically cycled sample (Fig. 5c). In contrast, the sample held at liquid nitrogen temperature for 300 min (Fig. 5d) displays a smaller pit diameter (8.3 \pm 2.9 μ m) compared to the as-cast sample. The evolution in pit morphologies is consistent with the observed passivation behavior in potentiodynamic polarization experiments. The CT2 sample with a wider Δ E shows smaller pits (Fig. 5e), whereas C2 sample with comparatively lower Δ E forms larger pits than the AC sample.

The trends of electrochemical behavior represented by the surface morphologies and the polarization experiments is also in accord with the observations in the EIS experiments in which the CT2 sample is characterized with a higher charge transfer resistance and impedance compared to the other samples (Fig. 6). These results collectively suggest the formation of a compact surface passivation in the MG samples exposed to cryogenic temperatures for long times. Cryogenic treatment has been reported to induce redistribution of atoms and reduction in atomic distance in metallic glass [42]. Due to the reduction in the effective atomic distance, the free volume is squeezed, making the

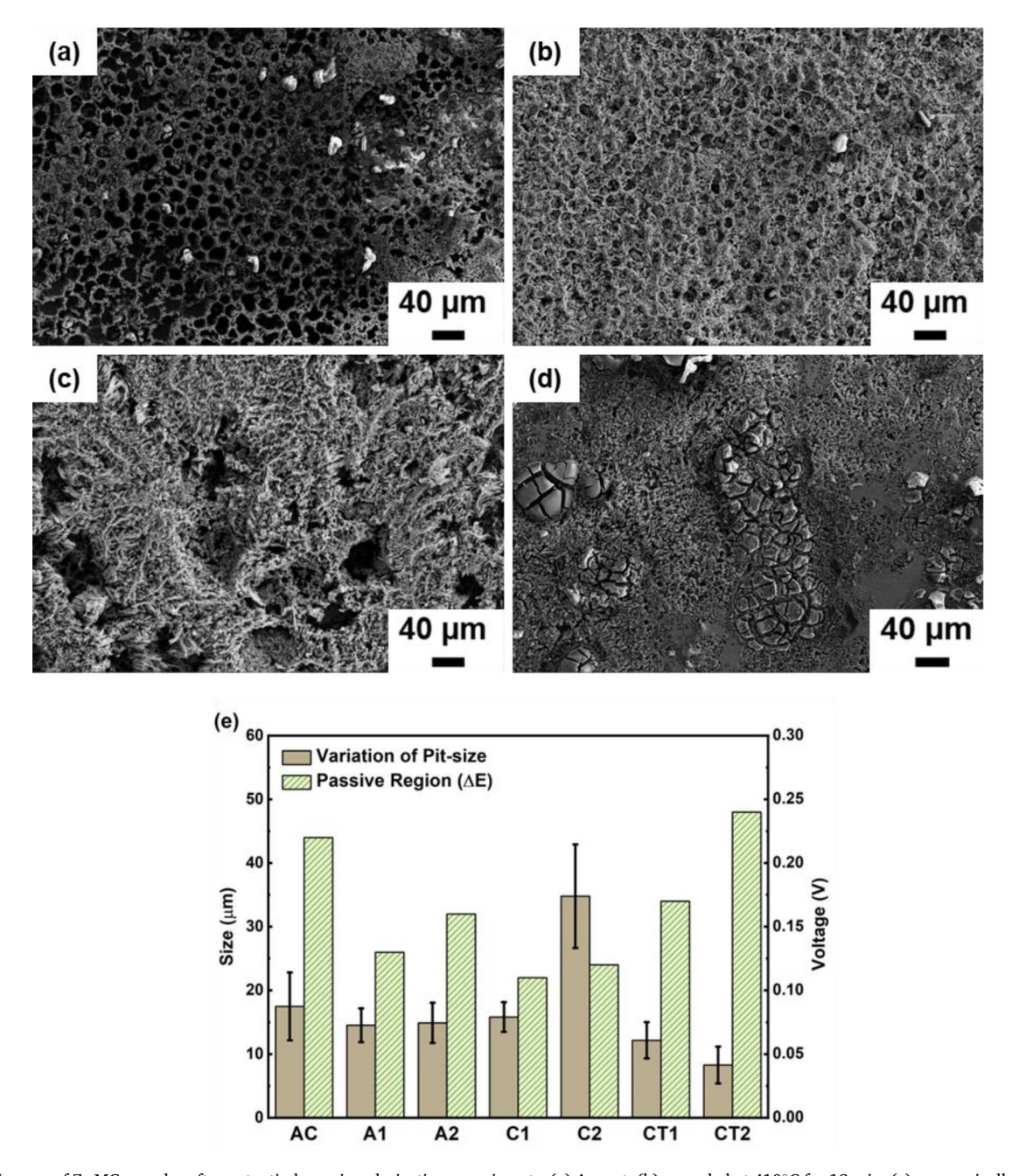


Fig. 5. SEM images of Zr-MG samples after potentiodynamic polarization experiments. (a) As-cast, (b) annealed at 410°C for 12 min, (c) cryogenically cycled for 30 times, and (d) held for 300 min at liquid nitrogen temperature. (e) Comparison of pit diameter after corrosion and the passive region observed in the potentiodynamic polarization traces for Zr-MG samples.

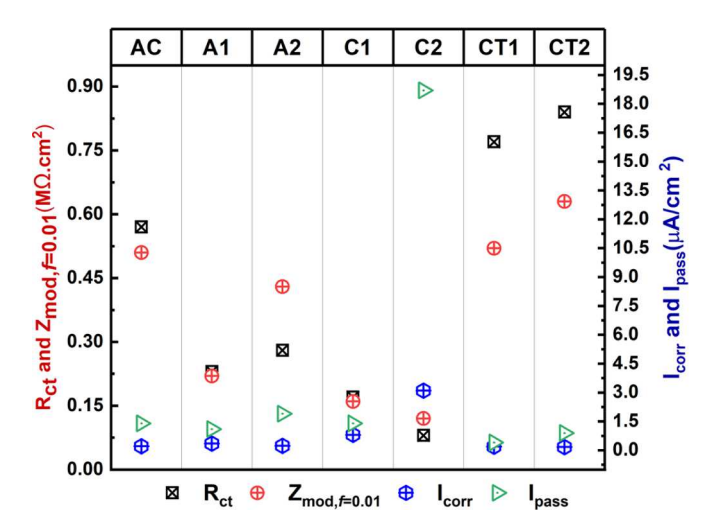


Fig. 6. Comparison between quantitative values of the crucial parameters achieved via EIS and potentiodynamic polarization experiments.

structure more uniform with a low potential energy [37,43]. Thus, it is reasonable to assume that the formation of stable passive film is promoted in homogeneous MG samples subjected to long cryogenic exposures. In contrast, the lower passivation of cryogenically cycled MG samples is associated with structural heterogeneities, which make the passive layer less dense. A porous passive layer is prone to penetration of chloride ions and pitting resulting in poor corrosion resistance [32]. Similarly, the above- T_g annealing induces heterogeneity in the form of the crystalline phases, which results in decreasing corrosion resistance. Therefore, the incorporation of structural heterogeneity by cryogenic cycling or partial crystallization used in improving the plasticity of MG is not effective in increasing the corrosion resistance. In contrast, an appropriate cryogenic holding can be used as a simple process to enhance the room temperature corrosion resistance of MGs.

4. Conclusions

The electrochemical properties of Zr₃₅Ti₃₀Cu_{8,25}Be_{26,75} metallic glass after cryogenic treatment and high temperature annealing were investigated in 3.5 wt.% NaCl. The results reveal that the corrosion resistance of metallic glass is improved after holding at the liquid nitrogen temperature due to decrease in structural heterogeneity. However, the commonly used cryogenic cycling for improvement of plasticity of metallic glasses deteriorates the corrosion resistance. The samples annealed above glass transition temperature also showed diminishing corrosion performance due to the formation of crystalline phases. Lower corrosion resistance of cryogenically cycled and high temperature annealed specimens is characterized by the low $Z_{mod,f=0.01}$ (Cycled: 0.12–0.16 M Ω -cm², Annealed: 0.23–0.28 M Ω -cm²) and ΔE (Cycled: 0.11-0.12 V, Annealed: 0.13-0.16 V) values compared to the as-cast (0.51 M Ω -cm² and ~0.21 V) sample. The EIS results show that the metallic glass samples held at cryogenic temperatures show higher electrochemical impedance compared to the as-cast, thermally annealed, and cryogenically cycled samples. High ΔE of 0.27 V for the cryogenically treated sample also indicates the formation of dense passive layer. The compact passivation layer results in smaller corrosion pits on the surface of cryogenically treated sample. Our results suggest that decreasing the structural or chemical heterogeneity by an appropriate cryogenic treatment is an effective approach to improve the corrosion resistance of Zr-based metallic glasses.

CRediT authorship contribution statement

Akib Jabed: Investigation, Data curation, Writing – original draft.

Golden Kumar: Supervision, Writing - review & editing.

Declaration of Competing Interest

None.

Data availability

No data was used for the research described in the article.

Acknowledgments

The work was supported by the National Science Foundation (NSF) through CMMI NSF-CAREER Award#1921435.

References

- M.D. Demetriou, M.E. Launey, G. Garrett, J.P. Schramm, D.C. Hofmann, W. L. Johnson, R.O. Ritchie, A damage-tolerant glass, Nat. Mater. 10 (2011) 123–128, https://doi.org/10.1038/nmat2930.
- [2] W. Song, X. Meng, Y. Wu, D. Cao, H. Wang, X. Liu, X. Wang, Z. Lu, Improving plasticity of the Zr46Cu46Al8 bulk metallic glass via thermal rejuvenation, Sci. Bull. 63 (2018) 840–844, https://doi.org/10.1016/j.scib.2018.04.021.
- [3] A. Jabed, M.M. Khan, J. Camiller, M. Greenlee-Wacker, W. Haider, I. Shabib, Property optimization of Zr-Ti-X (X= Ag, Al) metallic glass via combinatorial development aimed at prospective biomedical application, Surf. Coat. Technol. 372 (2019) 278–287, https://doi.org/10.1016/j.surfcoat.2019.05.036.
- [4] H.T. Zong, L.Y. Bian, J.Y. Cheng, G.H. Cao, C.Y. Kang, M. Li, Glass forming ability, thermal stability and elastic properties of Zr-Ti-Cu-Be-(Fe) bulk metallic glasses, Results Phys. 6 (2016) 1157–1160, https://doi.org/10.1016/j.rinp.2016.09.015.
- [5] S. Deng, H. Diao, Y. Chen, C. Yan, H. Zhang, A. Wang, Z. Hu, Metallic glass fiber-reinforced Zr-based bulk metallic glass, Scr. Mater. 64 (2011) 85–88, https://doi.org/10.1016/j.scriptamat.2010.09.014.
- [6] A. Jabed, Z.U. Rahman, M.M. Khan, W. Haider, I. Shabib, Combinatorial development and in vitro characterization of the quaternary Zr-Ti-X-Y (X-Y= Cu-Ag/Co-Ni) metallic glass for prospective bioimplants, Adv. Eng. Mater. 21 (2019), 1900726, https://doi.org/10.1002/adem.201900726.
- [7] K. Sun, R. Fu, X. Liu, L. Xu, G. Wang, S. Chen, Q. Zhai, S. Pauly, Osteogenesis and angiogenesis of a bulk metallic glass for biomedical implants, Bioact. Mater. 8 (2022) 253–266, https://doi.org/10.1016/j.bioactmat.2021.06.018.
- [8] Z. Hu, C.S. Meduri, R.S.J. Ingrole, H.S. Gill, G. Kumar, Solid and hollow metallic glass microneedles for transdermal drug-delivery, Appl. Phys. Lett. 116 (2020), 203703, https://doi.org/10.1063/5.0008983.
- [9] S. Jagdale, A. Jabed, S. Theeda, C.S. Meduri, Z. Hu, M. Hasan, G. Kumar, Review of thermoplastic drawing with bulk metallic glasses, Metals 12 (2022) 518, https:// doi.org/10.3390/met12030518. Basel.
- [10] J. Tang, L. Yu, J. Qiao, Y. Wang, H. Wang, M. Duan, M. Chamas, Effect of atomic mobility on the electrochemical properties of a Zr58Nb3Cu16Ni13Al10 bulk metallic glass, Electrochim. Acta 267 (2018) 222–233, https://doi.org/10.1016/j. electacta.2018.02.071.
- [11] C. Qin, W. Zhang, Q. Zhang, K. Asami, A. Inoue, Electrochemical properties and surface analysis of Cu–Zr–Ag–Al–Nb bulk metallic glasses, J. Alloys Compd. 483 (2009) 317–320, https://doi.org/10.1016/j.jallcom.2008.07.157.
- [12] N. Hua, Z. Liao, W. Chen, Y. Huang, T. Zhang, Effects of noble elements on the glass-forming ability, mechanical property, electrochemical behavior and tribocorrosion resistance of Ni-and Cu-free Zr-Al-Co bulk metallic glass, J. Alloys Compd. 725 (2017) 403–414, https://doi.org/10.1016/j.jallcom.2017.07.167.
- [13] D. Zander, B. Heisterkamp, I. Gallino, Corrosion resistance of Cu–Zr–Al–Y and Zr–Cu–Ni–Al–Nb bulk metallic glasses, J. Alloys Compd. 434 (2007) 234–236, https://doi.org/10.1016/j.jallcom.2006.08.112.
- [14] S. Guo, Z. Liu, K.C. Chan, W. Chen, H. Zhang, J. Wang, P. Yu, A plastic Ni-free Zr-based bulk metallic glass with high specific strength and good corrosion properties in simulated body fluid, Mater. Lett. 84 (2012) 81–84, https://doi.org/10.1016/j.matlet.2012.06.057.
- [15] N. Li, T. Xia, L. Heng, L. Liu, Superhydrophobic Zr-based metallic glass surface with high adhesive force, Appl. Phys. Lett. 102 (2013), 251603, https://doi.org/ 10.1063/1.4812480.
- [16] A. Tauseef, N. Tariq, J. Akhter, B. Hasan, M. Mehmood, Corrosion behavior of Zr-Cu-Ni-Al bulk metallic glasses in chloride medium, J. Alloys Compd. 489 (2010) 596-599, https://doi.org/10.1016/j.jallcom.2009.09.119.
- [17] W. Zhou, C. Zhang, M. Sheng, J. Hou, Glass forming ability and corrosion resistance of Zr-Cu-Ni-Al-Ag bulk metallic glass, Metals 6 (2016) 230, https://doi. org/10.3390/met6100230. Basel.
- [18] L. Liu, C. Qiu, Q. Chen, S. Zhang, Corrosion behavior of Zr-based bulk metallic glasses in different artificial body fluids, J. Alloys Compd. 425 (2006) 268–273, https://doi.org/10.1016/j.jallcom.2006.01.048.
- [19] Z. Qiu, Z. Li, H. Fu, H. Zhang, Z. Zhu, A. Wang, H. Li, L. Zhang, H. Zhang, Corrosion mechanisms of Zr-based bulk metallic glass in NaF and NaCl solutions, J. Mater. Sci. Technol. 46 (2020) 33–43, https://doi.org/10.1016/j.jmst.2019.10.043.

- [20] A. Gebert, P. Gostin, L. Schultz, Effect of surface finishing of a Zr-based bulk metallic glass on its corrosion behavior, Corros. Sci 52 (2010) 1711–1720, https://doi.org/10.1016/j.corsci.2010.01.027.
- [21] H. Tian, J. Qiao, H. Yang, Y. Wang, P. Liaw, A. Lan, The corrosion behavior of insitu Zr-based metallic glass matrix composites in different corrosive media, Appl. Surf. Sci. 363 (2016) 37–43, https://doi.org/10.1016/j.apsusc.2015.11.243.
- [22] A. Kawashima, K. Ohmura, Y. Yokoyama, A. Inoue, The corrosion behavior of Zr-based bulk metallic glasses in 0.5M NaCl solution, Corros. Sci. 53 (2011) 2778–2784, https://doi.org/10.1016/j.corsci.2011.05.014.
- [23] J.R. Scully, A. Gebert, J.H. Payer, Corrosion and related mechanical properties of bulk metallic glasses, J. Mater. Res. 22 (2007) 302–313, https://doi.org/10.1557/ imr 2007 0051
- [24] A. Wang, X. Chang, W. Hou, J. Wang, Corrosion behavior of Ni-based amorphous alloys and their crystalline counterparts, Corros. Sci. 49 (2007) 2628–2635, https://doi.org/10.1016/j.corsci.2006.12.017.
- [25] Y. Zhang, L. Yan, X. Zhao, L. Ma, Enhanced chloride ion corrosion resistance of Zr-based bulk metallic glasses with cobalt substitution, J. Non Cryst. Solids 496 (2018) 18–23, https://doi.org/10.1016/j.jnoncrysol.2018.05.005.
- [26] V.R. Raju, U. Kühn, U. Wolff, F. Schneider, J. Eckert, R. Reiche, A. Gebert, Corrosion behavior of Zr-based bulk glass-forming alloys containing Nb or Ti, Mater. Lett. 57 (2002) 173–177, https://doi.org/10.1016/S0167-577X(02)00725-5
- [27] O. Baulin, D. Fabrègue, H. Kato, T. Wada, S. Balvay, D.J. Hartmann, J.M. Pelletier, Be-free Zr-based metallic glass for biomedical applications, J. Non-Cryst. Solids 500 (2018) 78–83, https://doi.org/10.1016/j.jnoncrysol.2018.06.026.
- [28] J. Horton, D. Parsell, Biomedical potential of a zirconium-based bulk metallic glass, Mater Res Soc Symp Proc 754 (2002), https://doi.org/10.1557/PROC-754-CC1.5.
- [29] V. Hasannaeimi, M. Sadeghilaridjani, S. Mukherjee. Electrochemical and corrosion behavior of metallic glasses, MDPI: Basel, Switzerland, 2021, https://doi.org/ 10.3390/books978-3-03943-723-8.
- [30] R. Jindal, V. Raja, M.A. Gibson, M.J. Styles, T.J. Bastow, C. Hutchinson, Effect of annealing below the crystallization temperature on the corrosion behavior of Al–Ni–Y metallic glasses, Corros. Sci. 84 (2014) 54–65, https://doi.org/10.1016/j. corsci.2014.03.015.
- [31] N. Tailleart, R. Huang, T. Aburada, D. Horton, J. Scully, Effect of thermally induced relaxation on passivity and corrosion of an amorphous Al–Co–Ce alloy, Corros. Sci. 59 (2012) 238–248, https://doi.org/10.1016/j.corsci.2012.03.012.
- [32] J. Gu, Y. Shao, L. Shi, J. Si, K. Yao, Novel corrosion behaviors of the annealing and cryogenic thermal cycling treated Ti-based metallic glasses, Intermetallics 110 (2019), 106467, https://doi.org/10.1016/j.intermet.2019.04.010.

- [33] D. Liang, J.C. Tseng, X. Liu, Y. Cai, G. Xu, J. Shen, Investigation of the Structural Heterogeneity and Corrosion Performance of the Annealed Fe-Based Metallic Glasses, Materials 14 (2021) 929, https://doi.org/10.3390/ma14040929.
- [34] N. Hua, Z. Liao, Q. Wang, L. Zhang, Y. Ye, J. Brechtl, P.K. Liaw, Effects of crystallization on mechanical behavior and corrosion performance of a ductile Zr68Al8Ni8Cu16 bulk metallic glass, J. Non Cryst. Solids 529 (2020), 119782, https://doi.org/10.1016/j.inoncrysol.2019.119782.
- [35] S. Ketov, Y. Sun, S. Nachum, Z. Lu, A. Checchi, A. Beraldin, H. Bai, W. Wang, D. Louzguine-Luzgin, M. Carpenter, Rejuvenation of metallic glasses by non-affine thermal strain, Nature 524 (2015) 200–203, https://doi.org/10.1038/ nature14674.
- [36] J. Sun, M. Zhang, G. Ding, Y. Wang, M. Yu, F. Liu, Y. Sun, K. Zhu, X. Zhao, L. Liu, Hydrophobic and corrosion resistance properties of the electrochemically etched Zr-based bulk metallic glasses after annealing and cryogenic thermal cycling treatment, Colloids Surf. A Physicochem. Eng. Asp. 635 (2022), 128107, https:// doi.org/10.1016/j.colsurfa.2021.128107.
- [37] Zhao, K., Wang, N., Li, S., Zhou, G., Teng, X., Xu, J., Wang, Y., Li, J. Corrosion behavior of Ni62Nb332r5 bulk metallic glasses after annealing and cryogenic treatments, Chem. Phys. Mater. 2 (2023) 58-68, https://www.sciencedirect.com/science/article/pii/\$27725715220002137via%3Dihub.
- [38] G. Kumar, T. Ohkubo, K. Hono, Effect of melt temperature on the mechanical properties of bulk metallic glasses, J. Mater. Res. 24 (2009) 2353–2360, https://doi.org/10.1557/imr.2009.0272.
- [39] A. Jabed, C.S. Meduri, G. Kumar, Effect of time on the isothermal viscosity of metallic glass supercooled liquids, J. Alloys Compd. 863 (2021), 158067, https://doi.org/10.1016/j.jallcom.2020.158067.
- [40] I. Martin, T. Ohkubo, M. Ohnuma, B. Deconihout, K. Hono, Nanocrystallization of Zr41.2Ti13.8Cu12.5Ni10Be22.5 metallic glass, Acta Mater. 52 (2004) 4427–4435, https://doi.org/10.1016/j.actamat.2004.05.038.
- [41] N.S. Al-Mamun, A. Jabed, M. Noor-A-Alam, W. Haider, I. Shabib, Electrochemical response in physiological environments and mechanical properties of Ti51Si24Ni14Nb11 and Fe40Ti30Al18Si12 thin film metallic glasses, J. Non Cryst. Solids 575 (2022), 121209, https://doi.org/10.1016/j.inoncrysol.2021.121209.
- [42] M. Dokukin, N. Perov, E. Dokukin, A. Beskrovnyi, S. Zaichenko, Changes in the short-range order and magnetic properties of the amorphous magnetic metal alloy Fe78Cu1Nb4B3. 5Si13. 5 following cryogenic treatment, Phys. B Condens. Matter. 368 (2005) 267–272, https://doi.org/10.1016/j.physb.2005.07.020.
- [43] Y. Li, W. Zhang, C. Dong, A. Kawashima, A. Makino, P. Liaw, Effects of cryogenic temperatures on mechanical behavior of a Zr60Ni25Al15 bulk metallic glass, Mater. Sci. Eng. A 584 (2013) 7–13, https://doi.org/10.1016/j.msea.2013.06.063.